NMR studies in aqueous solution fail to identify significant conformational differences between the monomeric forms of two Alzheimer peptides with widely different plaque-competence, Aβ(1−40)^{ox} and Aβ(1−42)^{ox}

Roland Riek[1], Peter Güntert[1], Heinz Döbeli[2], Beat Wipf[2] and Kurt Wüthrich[1]

[1]*Institut für Molekularbiolgie und Biophysik, Eidgenössische Technische Hochschule-Hönggerberg, Zürich, Switzerland;* [2]*Hoffmann-La Roche Ltd, Basel, Switzerland*

NMR studies of amyloid β-peptides (Aβ) in aqueous solution provide a novel way in which to characterize the apparent Alzheimer's disease-related conformational polymorphism of Aβ. In the aqueous medium, neither of the polypeptides Aβ(1−40)^{ox} or Aβ(1−42)^{ox} (both of which contain a methionine sulfoxide at position 35) is folded into a globular structure, but they both deviate from random coil behavior by local conformational preferences of several short segments along the amino-acid sequence. Differences between the solution structures of Aβ(1−40)^{ox} and Aβ(1−42)^{ox} are indicated only by decreased flexibility of the region from about residue 32 to the C-terminus in Aβ(1−42)^{ox} when compared to Aβ(1−40)^{ox}. The lack of the observation of more extensive conformational differences between the two molecules is intriguing, considering that Aβ(1−42)^{ox} in aqueous solution has much higher plaque-competence than Aβ(1−40)^{ox}.

Keywords: Alzheimer's disease; aqueous solution; NMR; polypeptide; aggregation.

Alzheimer's disease (AD) is associated with the progressive accumulation of amyloid deposits in the brain and is identified by extracellular neuritic plaques and neurofibrillary tangles [1]. The major components of the plaques are polypeptides with 39−43 amino-acid residues, which are commonly referred to as 'amyloid β-peptides' (Aβ). Once it is cleaved from the much larger amyloid precursor protein (APP), which is a glycoprotein containing a single hydrophobic transmembrane region, Aβ has a high propensity for the formation of β-sheet-containing aggregates [2]. Production of Aβ and its aggregation and deposition appear to play a causative role in the onset of AD, and genetic factors or brain injuries may accelerate this process [3,4].

Aβ occurs as a heterogeneous ensemble of variant polypeptides in body fluids as well as in supernatants of cell cultures and brain amyloid deposits [5−7]. Heterogeneity occurs at both chain ends as well as in nonterminal sequence positions. For example, a substantial proportion of the peptides in brain deposits contain methionine in position 35 as sulfoxide (Aβ^{ox}) [6]. The heterogeneity at the C-terminus is of particular importance. About 90% of the molecules end at position 40 [Aβ(x−40)] and 10% at position 42 [Aβ(x−42)]. The extension by the dipeptide segment Ile41-Ala42 results in dramatically increased aggregation propensity when compared with the corresponding Aβ(x−40) [8,9]. The importance of this effect lies in the fact that some individuals with inherited early onset AD bear a mutation which increases the proportion of Aβ(x−42) [10−12].

In this paper we investigate whether the well documented, widely different competence for fibril formation of Aβ(1−40)^{ox} and Aβ(1−42)^{ox} [13] might be related to different conformational properties of the monomeric forms of the two polypeptides. NMR spectroscopy in aqueous solution was used to study the two polypeptides Aβ(1−40)^{ox} and Aβ(1−42)^{ox}, which were both generated in a dedicated procedure to yield monomeric species that could be dissolved in aqueous media and would thus retain their full plaque-competence [14]. This investigation extends previous studies of the solution structures of Aβ polypeptides, as these were mostly performed in solvent milieus that block aggregation, such as aqueous acids, trifluoroethanol, SDS, or hexafluoroisopropanol (reviewed in [15]). In the Discussion, the present results on Aβ(1−40)^{ox} and Aβ(1−42)^{ox} will be compared with data obtained from the only previous structural studies in aqueous solution, i.e. with the fragments Aβ(10−35) [16], Aβ(1−40) [16] and Aβ(12−28) [17], which all have a low competence for fibril formation when compared with Aβ(1−42)^{ox}.

MATERIALS AND METHODS

Sample preparation

Recombinant human Alzheimer's peptides were produced by expressing recombinant fusion proteins in *Escherichia*

coli. Aβ(1−40)^{ox} and Aβ(1−42)^{ox} peptides were liberated from their fusion tail by a procedure designed to generate monomeric peptides dissolved in 12 mM Tris/HCl [13,14]. ^{15}N-Labeled Aβ(1−40)^{ox} and Aβ(1−42)^{ox} peptides were produced by cultivating the *E. coli* cultures in minimal medium containing 0. 8 g·L$^{−1}$ of ^{15}N-ammonium chloride (Cambridge Isotope Laboratories) as the sole source of nitrogen, 5 g·L$^{−1}$ of glucose, 7 g·L$^{−1}$ of potassium phosphate (at pH 6. 8), 1 g·L$^{−1}$ of sodium chloride, 0.2 g·L$^{−1}$ of magnesium sulfate, 35 mg·L$^{−1}$ of thiamine, and trace elements were included by addition of FeCl$_3$, ZnCl$_2$, MnCl$_2$, CoCl$_2$, CaCl$_2$, CuCl$_2$, NiSo$_4$, Na$_2$MoO$_4$ and boric acid (further details on the addition of trace elements in [14]). In 10-L fermenter cultures, the pH was regulated with 4 M potassium hydroxide solution. A shake flask culture (0.5 L) in the above medium was grown overnight and used to inoculate the fermenter. Thus, dilution of ^{15}N by inoculum could be prevented. All other parameters were the same as described elsewhere [14]. In order to determine the extent of ^{15}N-labeling, the Aβ peptides were digested with endoproteinase lys-C prior to mass spectrometry analysis [18]. Based on the isotope pattern of the peptide fragments Aβ(1−16) and Aβ(17−28) a labeling degree of 97% was calculated.

NMR measurements were performed at standard conditions of pH 6.4 and $t = 8$ °C in 95% H$_2$O/5% ^{2}H$_2$O with 12 mM perdeuterated Tris/HCl buffer, unless stated otherwise. Typical polypeptide concentrations in the NMR samples were 0.1−1 mM.

NMR spectroscopy, resonance assignment and structure calculations

NMR measurements were performed on Bruker DRX500, DRX600, DRX750 and Varian Unity+400 spectrometers equipped with four radio frequency channels and triple resonance probes with actively shielded *z*-gradient coils. For data processing and spectral analysis we used the programs PROSA [19] and XEASY [20], respectively.

Resonance assignments and the input for structure calculations with Aβ(1−40)^{ox} were obtained by standard procedures from homonuclear 2D [^{1}H,^{1}H]-clean-TOCSY spectra [21] with $\tau_m = 10$ ms and $\tau_m = 90$ ms, and from [^{1}H,^{1}H]-NOESY spectra [22] recorded with $\tau_m = 200$ ms. The typical data size was 600×3072 complex points in the t_1 and t_2 time-domains, which was zero-filled to 2048×4096 data points. [^{15}N,^{1}H]-HSQC spectra [23] were recorded with a time domain data size of 350×2048 complex points, $t_{1,max}(^{15}N) = 200$ ms and $t_{2,max}(^1H) = 255$ ms. A 3D HNHA experiment [24] was measured with $35 \times 180 \times 2048$ complex points, which were zero-filled to $64 \times 512 \times 2048$ complex points, $t_{1,max}(^{15}N) = 20$ ms, $t_{2,max}(^1H) = 20$ ms and $t_{3,max}(^1H) = 255$ ms. With uniformly ^{15}N-labeled Aβ(1−40)^{ox}, ^{15}N{^{1}H}-NOE experiments [25] were measured in an interleaved way at ^{1}H resonance frequencies of 500 MHz and 750 MHz, using the procedure described by Dayie & Wagner [26]. The relaxation delay was 1.5 s. Proton saturation during 4 s was achieved by applying a train of 120-degree pulses in 20-ms intervals. The data set was recorded with $t_{1,max}(^{15}N) = 60$ ms and $t_{2,max}(^1H) = 290$ ms, and a time domain data size of 80×2048 complex points. With ^{15}N-labeled Aβ(1−42)^{ox}, [^{15}N,^{1}H]-HSQC and ^{15}N{^{1}H}-NOE experiments were measured at a ^{1}H resonance frequency of

750 MHz, using the same set-up as for Aβ(1−40)^{ox}. The ^{1}H chemical shifts are relative to 2,2-dimethyl-2-silapentane-5-sulfonate, sodium salt.

Diffusion measurements [27] were performed on a Varian Unity+400 spectrometer at 10 °C using H$_2$O as the calibration substance. A series of 40 spectra was recorded for each sample, using pulsed magnetic field gradient strengths varying from 5 to 30 G·cm$^{−1}$ to determine the diffusion constants, *D,* for the following compounds: Aβ(1−40)^{ox} (4.3 kDa; $D = 2.0 \times 10^{−6}$ cm^2·s$^{−1}$), the tetrapeptide H-Gly$_3$Ala-OH (0.3 kDa; $D = 1.1 \times 10^{−5}$ cm^2·s$^{−1}$), the nonapeptide H-Ala$_6$ProAla$_2$-OH (0.7 kDa; $D = 3.9 \times 10^{−6}$ cm^2·s$^{−1}$), the pheromone Er-22 from *Euplotes raikovi* (37 residues; 4 kDa; $D = 2.0 \times 10^{−6}$ cm^2·s$^{−1}$), the basic pancreatic trypsin inhibitor (58 residues; 6.5 kDa; $D = 1.2 \times 10^{−6}$ cm^2·s$^{−1}$), and a fusion protein of Aβ [14] (133 residues, 13.7 kDa; $D = 0.6 \times 10^{−6}$ cm^2·s$^{−1}$).

For a structural characterization of Aβ(1−40)^{ox}, sequence-specific ^{1}H NMR assignments were obtained using homonuclear techniques based on sequential NOEs [25]. Dihedral angle constraints were obtained with the program FOUND [28] on the basis of intraresidual and sequential NOEs, and of $^3J_{HN\alpha}$ couplings that were determined by inverse Fourier transformation of in-phase multiplets of [^{15}N,^{1}H]-HSQC cross peaks [29] and by the HNHA experiment [24]. The precision of the coupling constants is about 0.5 Hz. The calibration of NOE intensities vs. ^{1}H–^{1}H distances and the structure calculations were performed using the program DYANA [30]. A bundle containing the 20 DYANA conformers with the smallest residual target function values (see below) is used as a basis for discussions on the solution conformation of Aβ(1−40)^{ox}. Figure 5 was prepared with the program MOLMOL [31].

RESULTS

NMR observation of the aggregation behaviour of Aβ(1−40)^{ox} and Aβ(1−42)^{ox}

Aβ(1−40)^{ox} is soluble at millimolar concentrations in aqueous solution at pH values between 8.2 and 6.4. There was no evidence of precipitation in the sample for 15 h after the solution was prepared (Fig. 1): in fact, the ^{1}H NMR spectrum was unchanged after several weeks, suggesting that Aβ(1−40)^{ox} aggregation in aqueous solution is very slow. The monomeric state of Aβ(1−40)^{ox} in freshly prepared samples was further confirmed by the observation of a high-speed sedimentation profile in the analytical ultracentrifuge, and by NMR diffusion measurements (see Materials and methods). We observed some structured regions within the monomeric form of Aβ(1−40)^{ox} (see below), but did not detect any intermolecular NOEs that might indicate aggregation. Using different methods, similar conclusions on the solution behavior of Aβ(1−40)^{ox} were previously reported [13,14,16,32,33].

Rapid aggregation of Aβ(1−42)^{ox} was observed by the time change of the signal intensity in the NMR spectra (Fig. 1). With special care, Aβ(1−42)^{ox} solutions in H$_2$O can be prepared in such a way that a freshly prepared solution contains close to 100% monomers, as shown by observation of a high-speed sedimentation profile in the analytical ultracentrifuge, whereas electron micrographs of
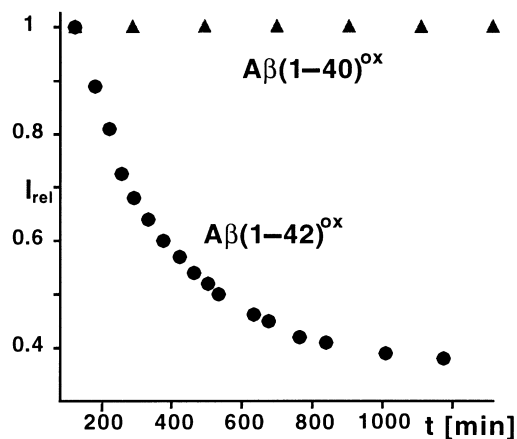
Fig. 1. Aggregation behaviour of Aβ(1–40)^{ox} and Aβ(1–42)^{ox}. The sum of the signal volumes with chemical shifts between 0.0 and 1.5 p.p.m. in the 1D ^{1}H NMR spectra of freshly prepared aqueous solutions of Aβ(1–40)^{ox} and Aβ(1–42)^{ox} is plotted vs. the time that has elapsed after the sample preparation. For both peptides signal intensity 1.0 corresponds to the first NMR measurement, which was recorded after the samples has been stored on ice for 2 h after the final preparation step. Aβ(1–40)^{ox} was measured at a concentration of 0.4 mM, pH 7.8 at 4 °C in 12 mM Tris/HCl buffer. Aβ(1–42)^{ox} was measured at a concentration of 0.1 mM, pH 8.2, 4 °C in 12 mM Tris/HCl buffer. Similar results were observed at different polypeptide concentrations and at lower pH values (see text).

Aβ(1–42)^{ox} taken after several days show fibril formation [13]. The signal decay in the NMR spectra vs. time is exponential (Fig. 1), as would be expected from the nucleation-dependent aggregation model for high Aβ concentrations [34,35]. As documented by Döbeli *et al.* [14] there is a strong batch-to-batch variability of the stability of Aβ(1–42) monomers in aqueous solution, so that the data in Fig. 1 represent a particular example rather than a standard value.

Resonance assignment and structure calculation of Aβ(1–40)^{ox}

Sequence-specific ^{1}H resonance assignments were obtained using sequential NOEs (Fig. 2) [25]. A listing of the ^{1}H
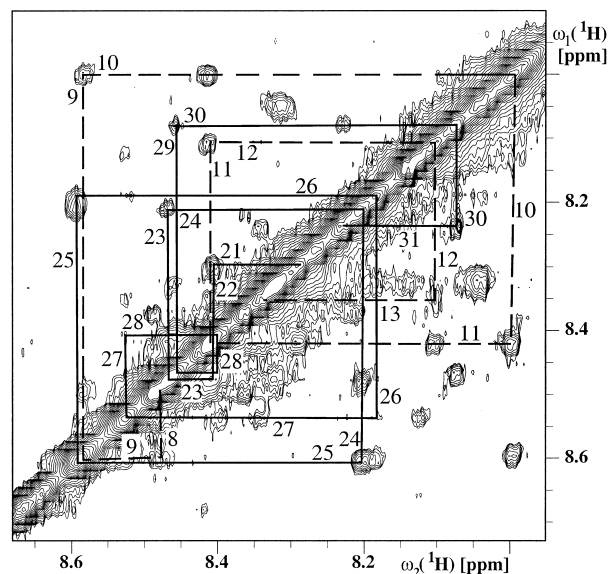
Fig. 2. Region of a [^{1}H,^{1}H]-NOESY spectrum of Aβ(1–40)^{ox} containing cross peaks between different amide protons. Sequential connectivities $d_{NN}(i,i + 1)$ linking the residues 8–13 (broken lines) and 21–31 (solid lines) are indicated. The [^{1}H,^{1}H]-NOESY spectrum [22] with a mixing time of $\tau_m = 200$ ms was measured at a proton frequency of 750 MHz (polypeptide concentration 1 mM, 8 °C, pH 6.4). The data size was 600×3072 complex points recorded in the t_1 and t_2 time domains, which was zero-filled to 2048×4096 points.

and ^{15}N chemical shifts has been deposited at the BMRB data bank (accession no. 5057). The resonance assignments are complete, except for H$^\varepsilon$ of Arg5, all resonances of His6, εH of His13 and His14, γCH$_3$ of Ile32, and εCH$_3$ of Met35. Two sets of resonances with relative intensity 2 : 1 were observed for the two diastereoisomers of the methionine sulfoxide residue. A similar observation has previously been reported for Aβ(1–40)^{ox} measured in aqueous SDS micelles [32]. Furthermore, a doubling of the resonances of the ^{15}N–^{1}H moieties of residues 31–39 was observed in the [^{15}N,^{1}H]-HSQC spectrum (data not shown), which is probably due to long-range effects from the methionine sulfoxide diastereoisomers in position 35.
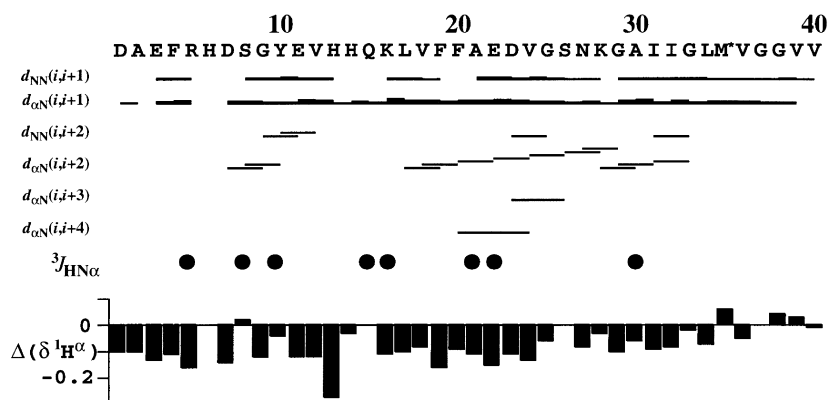
Fig. 3. Amino-acid sequence of Aβ(1–40)^{ox} (M* stands for methionine sulfoxide) and survey of selected NMR data. Sequential NOE connectivities $d_{NN}(i,i + 1)$, and $d_{\alpha N}(i,i + 1)$ are indicated with thick and thin black bars for strong and weak NOEs, respectively. Medium-range connectivities $d_{NN}(i,i + 2)$, $d_{\alpha N}(i,i + 2)$, $d_{\alpha N}(i,i + 3)$, and $d_{\alpha N}(i,i + 4)$ are shown by lines starting and ending at the positions of the residues related by the NOE. In the row labeled $^3J_{HN\alpha}$, filled circles denote residues with $^3J_{HN\alpha} < 6.0$ Hz. At the bottom the differences between α-proton chemical shifts and the corresponding random coil values (BMRB data bank) are shown (the random coil value for methionine was used for methionine sulfoxide).
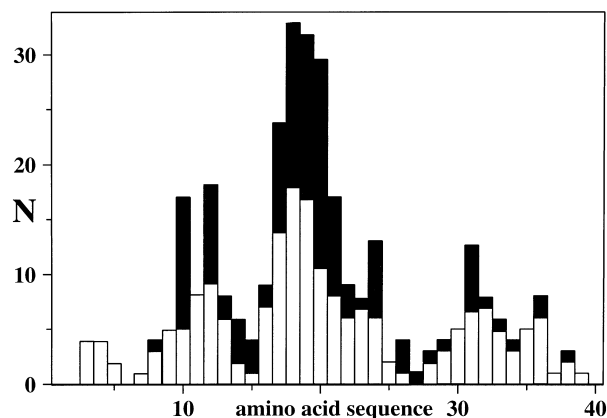
Fig. 4. Plot vs. the amino-acid sequence of Aβ(1−40)ox of the number of sequential and medium-range NOE distance constraints involving side chain hydrogens (white, sequential; black, medium-range).

A total of 628 NOESY cross peaks obtained at 750 MHz with a mixing time of 200 ms were assigned and integrated, resulting in 366 meaningful NOE upper limit distance constraints. Patterns of backbone−backbone NOE connectivities and small $^3J_{HN\alpha}$ scalar couplings are shown in Fig. 3, and Fig. 4 surveys the sidechain−backbone and sidechain−sidechain NOE connectivities.

The structure calculation presented in Table 1 was started with 50 randomized conformers, using an input of 366 NOE upper limit constraints and dihedral angle

constraints for 99 dihedral angles. The 20 DYANA conformers with the smallest target function values were subjected to restrained energy minimization using the AMBER all-atom force field [36] implemented in the program OPALP [37,38]. Deviations from ideal geometry are minimal, and similar AMBER energy values were obtained for all 20 conformers (Table 1).

Structural characterization of Aβ(1−40)ox

CD data indicate that Aβ(1−40)ox in aqueous solution is mainly a random coil [32]. We measured $^{15}N\{^1H\}$-NOEs to further investigate the flexibility of Aβ(1−40)ox in aqueous solution: typically, negative $^{15}N\{^1H\}$-NOE values are observed in flexibly extended polypeptides, and positive values of about 0.8−1.0 for structured parts of proteins [25]. For Aβ(1−40)ox, average values of 0.3 and 0.0 were measured at proton frequencies of 750 MHz (Fig. 5C) and 500 MHz (data not shown), respectively. On the basis of these data, a rotational correlation time of 1 ns was estimated for the $^{15}N-^1H$ bonds [25]. Thus, the $^{15}N\{^1H\}$-NOE data indicate that only the N-terminal residue and the C-terminal segment 37−40 have high flexibility. Aβ(1−40)ox is thus less flexible than, for example, the 100-residue 'tail' of the murine or Syrian hamster prion

Table 1. Statistics of the structure calculations of Aβ(1−40)ox with the programs DYANA and OPALP.

Parameter	Value
Upper limit NOE distance constraints	366
Number of constrained dihedral angles	99
Residual DYANA target function value[a,b]	$1.1 \pm 0.3 \text{ Å}^2$
Residual distance constraint violations[a]	
Number ≥ 0.1	7 ± 2
Maximum	0.13 ± 0.01 Å
Residual dihedral angle constraint violations[a]	
Number ≥ 2°	1 ± 1
Maximum	2.8 ± 0.6°
AMBER energies[a]	
Total	−1115 ± 75 kcal·mol⁻¹
Van der Waals	−2.2 ± 8.7
Electrostatic	−1472 ± 65
Rmsd from ideal geometry[a]	
Bond length	0.0077 ± 0.0003 Å
Bond angles	2.26 ± 0.13°
Rmsd to the averaged coordinates of N, Cα, and C′ of residues 16−24	0.7 Å

[a] The values given are the mean ± standard deviations among the 20 energy-minimized conformers with the smallest residual DYANA target function values before energy minimization. [b] Data before energy minimization.

Fig. 5. Plots vs. the amino-acid sequence enabling comparisons of the ^{15}N chemical shifts, the $^3J_{HN\alpha}$ coupling constants, and the $^{15}N\{^1H\}$-NOEs of Aβ(1−40)ox and Aβ(1−42)ox. (A) Differences of the backbone ^{15}N chemical shifts for nonterminal residues of Aβ(1−40)ox (black) and Aβ(1−42)ox (white) from their random coil values (BMRB data bank). (B) $^3J_{HN\alpha}$ scalar couplings of Aβ(1−40)ox (black) and Aβ(1−42)ox (white). Several sequentially adjoining values of $^3J_{HN\alpha} < 6$ Hz would be indicative of helical conformation, and 6 Hz $< ^3J_{HN\alpha} < 8$ Hz indicates random coil conformation [25]. G designates glycine residues. (C) $^{15}N\{^1H\}$-NOEs measured at a proton frequency of 750 MHz for Aβ(1−40)ox (black) and Aβ(1−42)ox (white). For residues labeled with *, no reliable information was obtained. '0' identifies residues for which a $^{15}N\{^1H\}$-NOE value of 0 was measured.
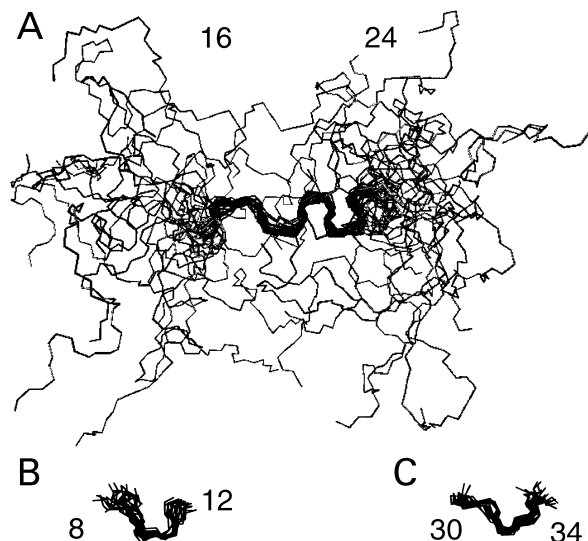
Fig. 6. Result of a structure calculation for Aβ(1−40)^{ox} repre-sented as a bundle of 20 energy-minimized DYANA conformers (see also Table 1). (A) Superposition of the complete polypeptide backbone chain for best fit of the backbone heavy atoms of residues 16−24. (B) Superposition of the backbone heavy atoms of residues 8−12. (C) Superposition of the backbone heavy atoms of residues 30−34.

proteins [39,40]. Based on these observations, some nonrandom structure was expected in Aβ(1−40)^{ox}. A structure calculation using an input of 465 restraints based on NOEs and ^{1}H–^{1}H scalar couplings (Figs 3 and 4, Table 1) indicates a trend to nonrandom structure for the following peptide segments: residues 20−24 form a helical turn (Fig. 6A); the segment 16−24 is characterized by numerous interresidual hydrophobic contacts, with NOEs between the sidechains of Leu17 and Phe19, Leu17 and Phe20, Val18 and Phe20, Phe19 and Ala21, Ala21 and Val24, and Phe19 and Val24; a clustering of residue 26 and the segment 29−36 is indicated by NOEs between methyl groups of Ile31, and the ^{1}H^N of Ser26, Gly33, and the side chain of Leu34; for residues 30−34, a locally well defined backbone conformation is indicated by the result of the structure calculation (Fig. 6C); for the segment 8−12 the result of the structure calculation suggests a turn-like nonrandom structure (Fig. 6B).

The algorithm GOR [41] indicates a propensity for helical structure formation for the entire segment of residues 11−24 in Aβ. The helical turn of residues 20−24 observed in aqueous solution is thus located in a region with predicted helix propensity, which is more clearly represented by the helix of residues 16−24 observed in an aqueous SDS micellar environment [15,32] and by even more extended helix formation in helix-inducing solvents [42,43]. The scarcity of medium-range backbone−backbone NOEs [25] (Fig. 3) indicates a low population of the local nonrandom conformational features of Aβ(1−40)^{ox} in aqueous solution. For example, NOE constraints $d_{\alpha\beta}(i,i+3)$, which are com-monly observed in α helices [25], are completely absent in Aβ(1−40)^{ox} (Fig. 3), and only one $d_{\alpha N}(i,i+3)$ NOE constraint was observed (Fig. 3). The observation of similar ^{1}H$^\alpha$ chemical shift deviations from their random coil values for nearly the entire Aβ(1−40)^{ox} sequence in aqueous

solution (Fig. 3) would be compatible with the assumption that the entire chain from residues 1−32 forms a non-random, rapidly interconverting conformational ensemble. With regard to the ^{1}H$^\alpha$ chemical shifts the previously mentioned peptide segments with indications of nonrandom structure do not stand out from the remainder of the poly-peptide segment 1−32, which would again be compatible with low populations of the molecular species with nonrandom structure. It is further seen that the structural features prevailing in a small proportion of Aβ(1−40)^{ox} in aqueous solution appear to be different from the nonrandom structure seen in other solvents. For example, while the residues 16−19 are helical in aqueous SDS, a more elon-gated structure seems to be favored in aqueous solution (Fig. 6A). Similarly, the highly hydrophobic segment of residues 28−36, which forms an α helix in aqueous SDS [32], has a more elongated structure in aqueous solution (Fig. 6C).

Comparison of Aβ(1−40)^{ox} with Aβ(1−42)^{ox}

Compared to Aβ(1−40)^{ox}, Aβ(1−42)^{ox} aggregates rapidly [14] (Fig. 1), highlighting the strong impact of residues Ile41 and Ala42 on the solution properties of Aβ. Only a limited number of NMR experiments have thus been feasible with Aβ(1−42)^{ox}, which nonetheless allow some comparisons of corresponding structural parameters in Aβ(1−42)^{ox} and Aβ(1−40)^{ox}. These include $^3J_{HN\alpha}$ scalar coupling constants (Fig. 5B), and ^{1}H^N and ^{15}N chemical shifts (Fig. 5A), which are so closely similar that no differ-ences between the average structures of the two peptides are indicated. ^{15}N{^{1}H}-NOEs (Fig. 5C), which yield data on the mobility of the peptide, reveal some differences. Higher ^{15}N{^{1}H}-NOEs values are observed for residues near the C-terminus of Aβ(1−42)^{ox} when compared with Aβ(1−40)^{ox} (Fig. 5C), showing that the addition of the two amino-acid residues 41 and 42 causes reduced flexibility of the entire segment 30−40 in Aβ(1−42)^{ox}.

DISCUSSION

In the recent years, it has become evident that the aggre-gation of Aβ may proceed via a different intermediate state, including monomers, small oligomers, nucleation cores, polymeric sheets, intermediate fibrils, protofilaments and multistranded fibrils as well as amorphous aggregates [44]. A selection of variant Aβ polypeptides that differ by amino-acid exchanges in position 35 or by variable C-terminal chain lengths, were shown to exhibit different aggregation properties as well as different proportions of these intermediates and a different fiber morphology [13]. With the present study we wanted to investigate whether these differences could also be related to different conformations of the monomeric Aβ polypeptides.

Aβ is thought to rearrange from a helical membrane-spanning conformation when it is part of intact APP via a so far unknown conformation in body fluids to an aggregated form with β sheet secondary structure, which is found in Alzheimer plaques. In helix-forming solvents, partially or nearly fully helical Aβ conformations have been reported [15,32,42,43], but in water there are only indications of small populations of local nonrandom structure (Figs 3−6). In previous NMR studies of Aβ(1−40) and Aβ(1−35) in

aqueous solution [16], a solution conformation was derived for Aβ(1−35). For Aβ(1−40), the $^1H^\alpha$ chemical shifts were found to be similar to the corresponding chemical shifts in Aβ(1−35), which led the authors to suggest that the two peptides have similar conformations. A comparison of the NMR data for Aβ(1−35) with those for Aβ(1−40)^{ox} indicates close similarities for the residues 17−21 (Fig. 6A). However, a helical turn of residues 20−24 that would correspond to the structure in Fig. 6A was not reported for Aβ(1−35), where in turn some long−range interactions of the residues 17−21 with Tyr10 and Met35 were documented, which are not observed in Aβ(1−40)^{ox}. These apparent structural differences might be a consequence of the different lengths of the constructs used, the different pH values, or the different oxidation states of Met35. In particular, the absence of long-range interactions between the central region of the polypeptide chain and Met35 in Aβ(1−40)^{ox} in aqueous solution might be related to the observation that the oxidation of Met35 has a strong destabilizing influence on the structure of micelle-associated Aβ [32]. Overall, considering that Aβ(1−42)^{ox} is much more plaque-competent than Aβ(1−40)^{ox}, it is intriguing that the present study detects a significant difference only in the reduced flexibility near the C-terminus of Aβ(1−42)^{ox} when compared with Aβ(1−40)^{ox}, but not in the NMR parameters that relate to the mean structure. We thus have an apparent correlation in that reduced plaque-competence [9,13] and increased flexibility of an extended segment near the C-terminus of monomeric Aβ in aqueous solution are both related to deletion of the hydrophobic residues Ile41 and Ala42.

The failure of the present comparative NMR measurements of ^{15}N and amide proton chemical shifts, and $^3J_{HN\alpha}$ coupling constants to detect differences between the average conformations of Aβ(1−40)^{ox} and Aβ(1−42)^{ox} shows that both polypeptides form a rapidly exchanging ensemble of predominantly extended chains, which probably include admixtures of species with locally nonrandom structure, as exemplified by data on Aβ(1−40)^{ox} (Figs 3, 4 and 6). This result leads to two conceptually different possible conclusions, which may possibly be further distinguished with the use of novel techniques in future investigations. One is that the widely different plaque competence of Aβ(1−40)^{ox} and Aβ(1−42)^{ox} results from different relative stabilities of intermediate forms found along the pathways leading to plaque formation (see above), and cannot be traced to conformational differences of the monomeric species. Alternatively, the different physiological properties of Aβ(1−40)^{ox} and Aβ(1−42)^{ox} could correlate either with the presently reported increased stiffness of the C-terminal chain end in Aβ(1−42)^{ox} (Fig. 5C), and/or with the presence of different lowly populated nonrandom monomeric conformers in the two peptides. The latter might not contribute measurably to the ensemble-averaged experimental values of chemical shifts and spin−spin coupling constans (Fig. 5A,B) but could, because of the different averaging, be manifested in the NOE data (Figs 3, 4, 5C and 6) [25]. Overall, the results of the present project emphasize the importance of conducting structural studies in near-physiological milieu rather than in 'structure-inducing' solvents, although the latter will usually provide technically more readily accessible and therefore more precise structural data.

REFERENCES

1. Iversen, L.L., Mortishire-Smith, R.J., Pollack, S.J. & Shearman, M.S. (1995) The toxicity *in vitro* of beta-amyloid protein. *Biochem. J.* **311**, 1−16.

2. Masters, C.L., Simms, G., Weinman, N.A., Muthaup, G., McDonald, B.L. & Beyreuther, K. (1985) Amyloid plaque core protein in Alzheimer disease and Down syndrome. *Proc. Natl Acad. Sci. USA* **82**, 4245−4249.

3. Price, D.L. & Sisodia, S.S. (1998) Mutant genes in familial Alzheimer's disease and transgenic models. *Annu. Rev. Neurosci.* **21**, 479−505.

4. Guo, Z., Cupples, L.A., Kurz, A., Auerbach, S.H., Volicer, L., Chui, H., Green, R.C., Sadovnick, A.D., Duara, R., DeCarli, C., Johnson, K., Go, R.C., Growdon, J.H., Haines, J.L., Kukull, W.A. & Farrer, L.A. (2000) Head injury and the risk of AD in the MIRAGE study. *Neurology* **54**, 1316−1323.

5. Wang, R., Sweeney, D., Gandy, S.E. & Sisodia, S.S. (1996) The profile of soluble amyloid beta protein in cultured cell media − detection and quantification of amyloid beta protein and variants by immunoprecipitation mass spectrometry. *J. Biol. Chem.* **271**, 31894−31902.

6. Näslund, J., Schierhorn, A., Hellman, U., Lannfelt, L., Roses, A.D., Thernberg, L.O., Silberring, J., Gandy, S.E., Winblad, B., Greengard, P., Nordstedt, C. & Terenius, L. (1994) Relative abundance of Alzheimer Aβ amyloid peptide variants in Alzheimer-disease and normal aging. *Proc. Natl Acad. Sci. USA* **91**, 8378−8382.

7. Tekirian, T.L., Saido, T.C., Markesbery, W.R., Russell, M.J., Wekstein, D.R., Patel, E. & Geddes, J.W. (1998) N-Terminal heterogeneity of parenchymal and cerebrovascular A beta deposits. *J. Neuropath. Exp. Neur.* **57**, 76−94.

8. Burdick, D., Soreghan, B., Kwon, M., Kosmoski, J., Knauer, M., Henschen, A., Yates, J., Cotman, C. & Glabe, C. (1992) Assembly and aggregation properties of synthetic Alzheimer's Aβ amyloid peptide analogs. *J. Biol. Chem.* **267**, 546−554.

9. Jarrett, J.T., Berger, E.P. & Lansbury, P.T. Jr (1993) The carboxy terminus of the beta amyloid protein is critical for the seeding of amyloid formation: implications for the pathogenesis of Alzheimer's disease. *Biochemistry* **32**, 4693−4697.

10. Citron, M., Oltersdorf, T., Haass, C., McConlogue, L., Hung, A.Y., Seubert, P., Vigo-Pelfrey, C., Lieberburg, I. & Selkoe, D.J. (1992) Mutation of the beta-amyloid precursor protein in familial Alzheimer's disease increases beta-protein production. *Nature* **360**, 672−674.

11. Suzuki, N., Cheung, T.T., Cai, X.D., Odaka, A., Otvos, L., Eckman, C., Golde, T.E. & Younkin, S. (1994) An increased percentage of long amyloid-beta protein secreted by familial amyloid-beta protein-precursor mutants. *Science* **264**, 1336−1340.

12. Querfurth, H.W., Wijsman, E.M., St. George-Hyslop, P.H. & Selkoe, D.J. (1995) Beta-APP messenger-RNA transcription is increased in cultured fibroplasts from the familial Alzheimer's disease-1 familiy. *Mol. Brain. Res.* **28**, 319−337.

13. Seilheimer, B., Bohrmann, B., Bondolfi, L., Müller, F., Stüber, D. & Döbeli, H. (1997) The toxicity of the Alzheimer's beta-amyloid peptide correlates with a distinct fiber morphology. *J. Struct. Biol.* **119**, 59−71.

14. Döbeli, H., Draeger, N., Huber, G., Jakob, P., Schmidt, D., Seilheimer, B., Stüber, D., Wipf, B. & Zulauf, M. (1995) A biotechnological method provides access to aggregation competent monomeric Alzheimer's 1–42 residue amyloid peptide. *Nat. Biotech.* **13**, 988–993.

15. Coles, M., Vicknell, W., Watson, A.A., Fairlie, D. & Craik, D.J. (1998) Solution structure of amyloid β-peptide (1–40)^{ox} in a water–micelle environement. Is the membrane-spanning domain where we think it is? *Biochemistry* **37**, 11064–11077.

16. Zhang, S., Iwata, K., Lachenmann, M.J., Peng, J.W., Li, S., Stimson, E.R., Lu, Y.-A., Felix, A.M., Maggio, J.E. & Lee, J.P. (2000) The Alzheimer's peptide Aβ adopts a collapsed coil structure in water. *J. Struct. Biol.* **130**, 130–141.

17. Jarvet, J., Damberg, P., Bodell, K., Eriksson, L.E.G. & Gräslund, A. (2000) Reversible random coil to beta-sheet transition and the early stage of aggregation of the Aβ (12–28) fragment from the Alzheimer peptide. *J. Am. Chem. Soc.* **122**, 4261–4268.

18. Grüninger-Leitch, F., Berndt, P., Langen, H., Nelboeck, P. & Döbeli, H. (2000) Identification of beta-secretase-like activity using a mass spectrometry-based assay system. *Nat. Biotech.* **18**, 66–70.

19. Güntert, P., Dötsch, V., Wider, G. & Wüthrich, K. (1992) Processing of multi-dimensional *NMR* data with the new software PROSA. *J. Biomol. NMR* **2**, 619–629.

20. Bartels, C., Xia, T., Billeter, M., Güntert, P. & Wüthrich, K. (1995) The program XEASY for computer-supported NMR spectral analysis of biological macromolecules. *J. Biomol. NMR* **6**, 1–10.

21. Griesinger, C., Otting, G., Wüthrich, K. & Ernst, R.R. (1988) Clean-TOCSY for ^{1}H spin system identification in macromolecules. *J. Am. Chem. Soc.* **110**, 7870–7872.

22. Kumar, A., Ernst, R.R. & Wüthrich, K. (1980) A two-dimensional nuclear Overhauser enhancement (2D NOE) experiment for the elucidation of complete proton–proton cross-relaxation networks in biological macromolecules. *Biochem. Biophys. Res. Comm.* **95**, 1–6.

23. Bodenhausen, G. & Ruben, D. (1980) Natural abundance ^{15}N NMR by enhanced heteronuclear spectroscopy. *Chem. Phys. Lett.* **69**, 185–188.26.

24. Vuister, G.W. & Bax, A. (1993) Quantitative J correlation – a new approach for measuring homonuclear 3-bond *J* (H^{N}H^α) coupling constants in ^{15}N-enriched proteins. *J. Am. Chem. Soc.* **115**, 7772–7777.

25. Wüthrich, K. (1986) *NMR of Proteins and Nucleic Acids*. Wiley, New York.

26. Dayie, K.T. & Wagner, G. (1994) Relaxation-rate measurements for ^{15}N–^{1}H groups with pulsed-field gradients and preservation of coherence pathways. *J. Mag. Reson. A* **111**, 121–126.

27. Stejskal, E.O. & Tanner, J.E. (1965) Spin diffusion measurements: spin echoes in the presence of a time-dependent field gradient. *J. Chem. Phys.* **42**, 288–292.

28. Güntert, P., Billeter, M., Ohlenschläger, O., Brown, L.R. & Wüthrich, K. (1998) Conformational analysis of protein and nucleic acid fragments with the new grid search algorithm FOUND. *J. Biomol. NMR.* **12**, 543–548.

29. Szyperski, T., Güntert, P., Otting, G. & Wüthrich, K. (1992) Determination of scalar coupling constants by inverse Fourier transformation of in-phase multiplets. *J. Magn. Reson.* **99**, 552–560.

30. Güntert, P., Mumenthaler, C. & Wüthrich, K. (1997) Torsion angle dynamics for NMR structure calculation with the new program DYANA. *J. Mol. Biol.* **273**, 283–298.

31. Koradi, R., Billeter, M. & Wüthrich, K. (1996) MOLMOL: a program for display and analysis of macromolecular structures. *J. Mol. Graphics* **14**, 51–55.

32. Watson, A.A., Fairlie, D.P. & Craik, D.J. (1998) Solution structure of methionine-oxidized amyloid β-peptide (1–40). Does oxidation affect conformational switching? *Biochemistry* **37**, 12700–12706.

33. Tseng, B.P., Esler, W.P., Clish, C.B., Stimson, E.R., Ghilardi, J.R., Vinters, H.V., Mantyh, P.W., Lee, J.P. & Maggio, J.E. (1999) Deposition of monomeric, not oligomeric, Aβ mediates growth of Alzheimer's disease amyloid plaques in human brain preparations. *Biochemistry* **38**, 10424–10431.

34. Jarrett, J.T. & Lansbury, P.T. Jr (1993) Seeding 'one-dimensional crystallization' of amyloid: a pathogenic mechanism in Alzheimer's disease and scrapie? *Cell* **92**, 1055–1058.

35. Lomakin, A., Chung, D.S., Benedek, G.G., Kirschner, D.A. & Teplow, D.B. (1996) On the nucleation and growth of amyloid beta-protein fibrils: detection of nuclei and quantitation of rate constants. *Proc. Natl Acad. Sci. USA* **93**, 1125–1129.

36. Weiner, P.K., Kollman, P.S., Nguyen, D.T. & Case, D.A. (1986) An all-atom force field for simulations of proteins and nucleic acids. *J. Comp. Chem.* **7**, 230–252.

37. Luginbühl, P., Güntert, P., Billeter, M. & Wüthrich, K. (1996) The new program OPAL for molecular dynamics simulations and energy refinements of biological macromolecules. *J. Biomol. NMR.* **8**, 136–146.

38. Koradi, R., Billeter, M. & Güntert, P. (2000) Point-centered domain decomposition for parallel molecular dynamics simulation. *Comp. Phys. Commun.* **124**, 139–147.

39. Riek, R., Hornemann, S., Wider, G., Glockshuber, R. & Wüthrich, K. (1997) NMR characterization of the full length recombinant murine prion protein, mPrP (23–231). *FEBS Lett.* **413**, 282–288.

40. Donne, D.G., Viles. J.H., Groth, D., Mehlhorn, I., James, T.L., Cohen, F.E., Prusiner, S.B., Wrigth, P.E. & Dyson, H.J. (1997) Structure of the recombinant full-length hamster prion protein PrP (29–231): the N terminus is highly flexible. *Proc. Natl Acad. Sci. USA* **94**, 13452–13457.

41. Gibrat, J.F., Garnier, J. & Robson, B. (1987) Further developments of protein secondary structure prediction using information theory. New parameters and consideration of residue pairs. *J. Mol. Biol.* **198**, 425–443.

42. Shao, H., Jao, S., Ma, K. & Zagorski, M.G. (1999) Solution structures of micelle-bound amyloid beta (1–40) and beta (1–42) peptides of Alzheimer's disease. *J. Mol. Biol.* **285**, 755–773.

43. Crescenzi, O., Tomaselli, S., Guerrini, R., Salvadori, S.D., Ursi, A.M. & Picone, D. (2001) Solution structure of amyloid β-peptide (1–42). *Abstracts of the EURESCO Conference on NMR in Molecular Biology, Karrebaeksminde, Denmark, June 9–14*, p. 101. Euresco Conferences, Strasbourg.

44. Bohrmann, B., Adrian, M., Dubochet, J., Kuner, P., Müller, F., Huber, W., Nordstedt, C. & Döbeli, H. (2000) Self-assembly of β-amyloid 42 is retraded by small molecular ligands at the stage of structrual intermediates. *J. Struct. Biol.* **130**, 232–246.